Proceedings of the ASME 5th Joint US-European Fluids Engineering Summer Conference
FEDSM2018
July 15-20, 2018, Montreal, Canada

FEDSM2018-83296

COMPUTATIONAL MODELING OF FLOW RATE MEASUREMENTS USING AN ORIFICE FLOW METER

YiQin Xu*
School of Engineering of Matter, Transport and Energy
Arizona State University
Tempe, AZ, 85255
E-mail: yiqinxu@asu.edu

Daniel Coxe
School of Engineering of Matter, Transport and Energy
Arizona State University
Tempe, AZ, 85255
E-mail: dcoxe@asu.edu

Yulia Peet
School of Engineering of Matter, Transport and Energy
Arizona State University
Tempe, AZ, 85255
E-mail: ypeet@asu.edu

Taewoo Lee
School of Engineering of Matter, Transport and Energy
Arizona State University
Tempe, AZ, 85255
E-mail: ATTWL@asu.edu

ABSTRACT

This study is concerned with understanding and improvement of mass flow rate measurement uncertainty and errors encountered at low flow rates and start-up in commercially available flow rate measurement devices, such as orifice flow meters. The flow through a typical cylindrical flange-tapped orifice flow meter is modeled computationally so the actual mass flow rate is known a-priori. Empirical predictions from the reading of "virtual" pressure sensors are compared with the actual flow rate and the measurement errors are quantified and analyzed. Commercial code ANSYS-Fluent is compared in this study to the in-house high-fidelity spectral-element solver Nek5000, so that conclusions about the applicability of a commercial code to the calculations of measurement uncertainty in the orifice flow meters can be made.

NOMENCLATURE

D Meter tube internal diameter.
d Orifice plate bore diameter.
t Thickness of the orifice plate.
l1 Upstream meter tube length.
l2 Downstream meter tube length.
q_m Mass flow rate from empirical equation.
$\bar{q}_m$ Corrected mass flow rate from empirical equation.
C_d Orifice plate coefficient of discharge.
E_v Velocity of approach factor.
Y Expansion factor.
g_c Dimensional conversion constant.
ρ Fluid density.
μ Fluid dynamic viscosity.
Δp Orifice differential pressure.
π Universal constant.
Re_D Pipe Reynolds number.
Re Reynolds number.
β Diameter ratio.
Q_m Mass flow rate from simulation.
e Napierian constant.
SCFH Standard cubic feet per hour.

*Address all correspondence to this author

INTRODUCTION

Differential-pressure flow meter is a device used to measure flow rate from pressure drop through a constriction in a pipe such as an orifice, venturi tube, V-cone, etc, and it contributes to at least 40% of industrial flow meters in use as of 2015 in various industries, e.g. water, natural gas or oil industry [1] . The most popular geometry for its accurate measurement is an orifice plate which is a thin plate with a hole in it. Orifice plate is small, simple, easy to install or remove. Also, compared to some other, more advanced measuring technologies, such as ultrasonic flow meter [2], it is relatively cost effective and easy to maintain. There are mainly three types of orifice plates - concentric, segmental and eccentric based upon the measuring objectives, e.g. a segmental orifice is better used for colloidal and slurry flow, while eccentric one is better suited for solids, oil containing water and wet streams. For liquids, gas and vapor, 80 percent of measurements choose square-edged concentric orifice, as per [3].

For a sharp-edged orifice flow meter with corresponding tappings, mass flow rate is obtained based on the potential flow model from Bernoulli's theorem [1], and in practice, a discharge coefficient multiplies the expression from Bernoulli's equation, to take account for the difference between real and ideal (potential) flow rate. One of the most recognized expressions for a discharge coefficient is the Reader-Harris/Gallagher (RG) equation (1990, 1998), that is accepted as a gold standard in American Gas Association (AGA) and American Petroleum Institute (API) publications and is commonly used in many commercial flowmeter devices. The Reader-Harris/Gallagher (RG) equation was developed through an extensive regression data analysis obtained from four working fluids at different operational regimes and for different orifice plate geometries [4]. It gives an advantage of being a generalized expression suitable for many different configurations, but it is calibrated only for high Reynolds number regimes ($Re > 4000$) and fully-developed flow conditions. While RG equation is inaccurate at low Reynolds number regimes, it is still being used by industry practitioners at the absence of an alternative expression, and due to unawareness. This mis-use of the standard RG equation at low flow rates leads to large uncertainties in the prediction of the flow rate in industrial operations, and consequently in the estimation of the consumption of the working fluid. In the UK, for example an estimated uncertainty of natural gas consumption is about £25 billion per year, which is associated with a monetary equivalent of metering uncertainty of £250 million per year. Since industrial operations at low Reynolds numbers are unavoidable and ubiquitous (for example, during a start-up or shut-down of equipment), these uncertainties, and the measurement errors at low Reynolds numbers must be minimized.

The current paper is devoted to an investigation of flow rate measurement uncertainties at low Reynolds numbers via a computational simulation framework, where the flow rate measurements can be obtained from "virtual" (numerical) pressure sensors at the wall and compared to an actual flow rate (supplied as inflow conditions), from which the measurement error can be deduced. We indeed confirm the low accuracy of the RG equation at low flow rates, quantify the errors versus the Reynolds number at two flow conditions, and propose a low-Reynolds number correction for a given orifice geometry, that recovers the actual flow rate without an error. The correction is based on the correlation of the simulation data with the "virtual" orifice pressure reading at low flow rates at a certain flow condition. We also investigate the flow measurement uncertainties in the presence of unsteady velocity ramp conditions, simulating the unsteady effects of start-up an shut-down of equipment during the operations, and relate the measurement errors to transient unsteady vortex systems formed behind the orifice plate in these regimes [5, 6]

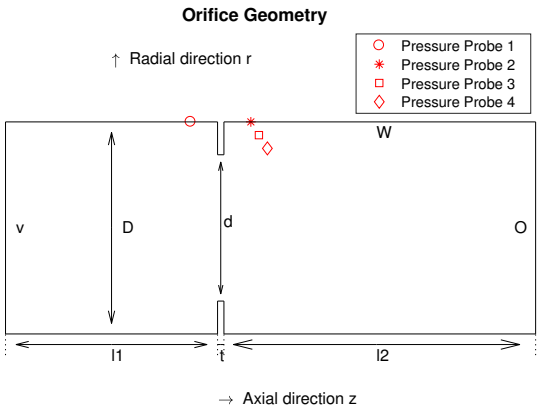

FIGURE 1. THE SKETCH OF THE CROSS SECTION OF A NATURAL GAS ORIFICE FLOW METER.

MODELING FRAMEWORK

Geometry of the Orifice Flow Meter

The simulation geometry is based on a realistic natural gas orifice flow meter. An orthographic projection of its cross section is illustrated in Fig. 1. D = 0.2 (m) is the meter pipe's internal diameter, d=0.139 (m) is the orifice bore, t=0.006 (m) is the thickness of the orifice plate, and l1, l2 are the upstream and downstream pipe lengths, respectively. Two values of the upstream distance l1, 2.5D and 5D, are used and compared in this paper, while the downstream distance l2 is fixed at 7.75D. The boundary conditions are also illustrated in Fig. 1, where v represents the inlet boundary, O is an outlet boundary and W is non-slip wall boundary. A plug flow or a laminar parabolic profile with a specified mass flux is supplied at the inlet boundary. To avoid a negative local flux at the outflow, which would result in numeri-

cal instabilities, the downstream meter tube length was increased and a divergence function [7] was imposed on the boundary.

The geometry is slightly modified in ANSYS-Fluent. All major dimensions are kept the same D = 0.2 (m) and d=0.139 (m). However, the upstream length l1 is 3D and l2 is 6D. ANSYS is very robust at dealing with reversed flow at the outlet and thus faced no divergence issues with this geometry.

Pressure Probes 1 and 2 are placed 25.4 (mm) upstream and downstream as the flange-tapped orifice meter on the walls of the pipe, and are going to be used in this paper as the baseline measurement locations. In practice, the pressure sensors have finite dimensions and might end up measuring the flow pressure at a location that is off-set from the wall. In order to evaluate uncertainty in the measurements to the location of the downstream pressure sensor, two additional downstream pressure probes were placed: Probe 3 at a distance 33 (mm) downstream of the orifice and 12.5 (mm) from the wall, and Probe 4 at a distance 41 (mm) downstream of the orifice and 25 (mm) from the wall. Uncertainty in the downstream probes were deemed to be more substantial, due to a potential flow modification at the orifice exit caused by separation and vortex shedding, while the uncertainty in the upstream probe was not investigated in this study.

Computational Fluid Dynamics Solvers

The simulation results of this paper are based primarily on a high-order spectral element code Nek5000. Additionally, some results from commercial code ANSYS-Fluent 18.2 are used for the purpose of comparison.

Nek5000 Spectral element code Nek5000 [8] has been continually developed for more than 30 years. It is a fast, scalable and highly efficient high-order solver for computational fluid dynamics problems. Spectral element method (SEM) is similar in its form to finite element methods, but it utilizes high-order basis functions, specifically, high-order polynomials associated with the Gauss-Legendre-Lobatto quadrature points. It leverages the chosen polynomial approximation for a tensor-product efficiency that allows for a fast convergence.

The numerical scheme used in Nek5000 solves incompressible Navier-Stokes equations with a backward-differentiation formula with time step δt and an explicit extrapolation for the convective term. Pressure p and velocity $\mathbf{u}$ are decoupled though a standard splitting operation in a following semi-discrete representation:

$$\begin{aligned}\frac{\beta_k \bar{\mathbf{u}}}{\delta t} - \frac{\mu}{\rho}\Delta\bar{\mathbf{u}} = -\sum_{j=1}^{k}\frac{\beta_{k-j}}{\delta t}\mathbf{u}^{n+1-j} \\ -\sum_{j=1}^{k}\alpha_j(\mathbf{u}\cdot\nabla\mathbf{u})^{n+1-j} - \frac{\nabla\bar{p}^{n+1}}{\rho},\end{aligned} \tag{1}$$

$$\Delta(p^{n+1} - \bar{p}^{n+1}) = \nabla\cdot(\frac{\beta_k\bar{\mathbf{u}}}{\delta t}), \tag{2}$$

$$\mathbf{u}^{n+1} = \bar{\mathbf{u}} - \frac{\delta t}{\beta_k}\nabla\cdot(p^{n+1} - \bar{p}^{n+1}). \tag{3}$$

Here n is the time step index, ρ is the density of the fluid, μ is the dynamic viscosity, $\bar{\mathbf{u}}$ and $\bar{p}^{n+1} = 2p^n - p^{n-1}$ are the intermediate velocity and extrapolated pressure at $n+1$ time step, respectively. The terms β and α represent the coefficients of the backward difference and extrapolation schemes of a given convergence order k. In the current study, k is set to 2, corresponding to a second order accuracy in time both for velocity and for pressure [8, 9].

Eqns. (1), (2), (3) are spatially discretized in a spectral-element $P_N - P_{N-2}$ formulation. The velocity and the pressure are represented in the polynomials spaces X^N and Y^{N-2}, which are finite-dimensional subsets of $\mathscr{H}_0^1(\Omega)$ and $L^2(\Omega)$, where Ω is the computational domain [8, 9]. The discretized approximation of velocity for example in an element Ω^e would be $\boldsymbol{u}(\boldsymbol{x})|_{\Omega^e} = \sum_{i,j,k=1}^{N}\boldsymbol{u}^e_{ijk}h_i(r)h_j(s)h_k(\zeta)$. Here $h_i(r)$, $i = 0,\ldots,N$ are the basis functions in the form of Lagrange polynomials based on Gauss-Legendre-Lobatto quadrature points, ξ_j, such that $h_i(\xi_j) = \delta_{ij}$. In that way, SEM provides exponential convergence of the solution with the degree of the interpolating polynomials N [8, 9], and in this paper, $N = 7$ has been employed. The computations with Nek5000 were run in Direct Numerical Simulations (DNS) regime or Large Eddy Simulations (LES) regime, depending on the Reynolds number. The numerical grid for all Reynolds numbers comprised of 375 elements in the pipe cross-section (on average, the cross-sectional area upstream of the orifice was slightly less refined, while the cross-sectional area downstream of the orifice was slightly more refined), with 150 elements across the streamwise length of the pipe, giving 56190 elements, and approximately 19 mln. grid points in total. To achieve stabilization at higher Reynolds numbers, an explicit modal filtering with the weight $\gamma = 0.01$ was applied to the last two modes of the polynomial approximation [10], which can also be thought of as an implicit subgrid-scale model in Large Eddy Simulations [11].

ANSYS-Fluent ANSYS-Fluent is a commercially available Computational Fluid Dynamics solver suite. It has a multitude of different solver formulations for both incompressible (pressure-based, decoupled velocity and pressure) and compressible (density-based, coupled velocity and pressure) as well as transient and steady-state formulations. Given the relatively slow speed of the flow and to ensure comparability, an incompressible transient solver was implemented.

The specific algorithm was the SIMPLE-C [12] (Semi-IMplicit Pressure Linked Equations-Consistent) algorithm. This

is a second order accurate algorithm in space and time. The SIMPLE-C algorithm is a predictor correct algorithm built on a staggered grid. The velocity components are calculated on the cell faces, while the pressure is always calculated at the cell center to limit the potential of checker-boarding dynamics where adjacent cells become decoupled.

Typically, commercial codes are run in a Reynolds-Averaged Navier Stokes (RANS) regime, which has the benefits of significant computational savings. In addition to offering multiple formulations for solving the Navier-Stokes Equations, ANSYS-Fluent offers many different models of turbulence. In the interest of maintaining conformity with standard industrial practice, the K-ω SST model [13] with Low Reynolds number correction was chosen for the current simulations. The simulations with ANSYS-Fluent described in this paper were done in the DNS setting (without the turbulence model) for $Re < 2000$, and in the RANS setting (with K-ω SST model turned on) for higher Reynolds numbers, on a grid that consisted of 393100 total elements amounting to approximately 1.5 mln grid nodes. The simulations with ANSYS-Fluent were performed in this paper to judge the ability of conventional low-fidelity approaches to model complex unsteady flows associated with sharp orifices in flow measurement devices as compared to a DNS research code employing high-order methods.

ORIFICE METER MASS FLOW EQUATION

The orifice flow meter uses only the measurements from the pressure sensors upstream and downstream of the orifice. Given a pressure difference, the mass flow is calculated based on a discharge coefficient equation developed by Reader-Harris/Gallagher (1990) for concentric, square-edged, and flange-tapped orifice meters as reported in American Gas Association Report No.3 Part 1 [4]. There are other equations such as Reader-Harris/Gallagher (1998) and PR14 [1] as well, but here we would present Reader-Harris/Gallagher (1990) in detail. The equation is representative of any major working fluid including natural gas (which this study considers), various orifice configurations, pipe diameters greater than 50 (mm), and an orifice plate bore diameter greater than 11.4 (mm) [4]. But the measuring system should be calibrated to meet the similarity of the reference conditions with that obtained in a laboratory environment. The equation is

$$q_m = C_d E_v Y (\frac{\pi}{4}) d^2 \sqrt{2 g_c \rho \Delta p}, \tag{4}$$

where q_m is mass flow rate, C_d is orifice plate coefficient of discharge, E_v is the velocity of approach factor, Y is the expansion factor, g_c is the dimensional conversion constant, ρ is the working fluid density and Δp is orifice differential pressure. The current equation is calibrated using a fully developed approach flow.

The working fluid of this paper is natural gas where its density ρ= 1 ($\mathrm{kg\,m^{-3}}$) and dynamic viscosity μ=10^{-5} ($\mathrm{kg\,m^{-1}\,s^{-1}}$). These fluid properties are considered constant in the simulation.

In Eqn. (4), with the exception of the discharge coefficient C_d and measured values Δp, all values are predetermined. The velocity of approach factor $E_v = \frac{1}{\sqrt{1-\beta^4}}$ with $\beta = \frac{d}{D}$ being the diameter ratio. The expansion factor $Y = 1$ as the flow is considered incompressible. The dimensional conversion constant g_c is 1 ($\mathrm{kg\,m\,N^{-1}\,s^{-2}}$).

The discharge coefficient C_d for an orifice meter with flange taps and diameter ratio β of 0.1-0.75 is determined by:

$$C_d = C_i(FT) + 0.000511(\frac{10^6\beta}{Re_D})^{0.7} + (0.021 + 0.0049A)\beta^4 C, \tag{5}$$

$$C_i(FT) = C_i(CT) + TapTerm,$$
$$C_i(CT) = 0.5961 + 0.0291\beta^2 - 0.229\beta^8 + 0.003(1-\beta)M_1,$$

$$TapTerm = Upstrm + Dnstrm,$$
$$Upstrm = (0.0433 + 0.0712e^{-8.5L_1} - 0.1145e^{-6L_1})(1 - 0.23A)B,$$
$$Dnstrm = -0.0116(M_2 - 0.52M_2^{1.3})\beta^{1.1}(1 - 0.14A),$$

$$B = \frac{\beta^4}{1-\beta^4},$$
$$M_1 = max(2.8 - \frac{D}{N_4}, 0),$$
$$M_2 = \frac{2L_2}{1-\beta},$$
$$A = (\frac{19000\beta}{Re_D})^{0.8},$$
$$C = (\frac{10^6}{Re_D})^{0.35},$$

where e is the Napierian constant, N_4 is the tap location, L_1, L_2 are the dimensionless corrections for the tap location. In this study, we use $N_4 = 24.5(\mathrm{mm})$, and $L_1 = L_2 = N_4/D$, which corresponds to the pressure Probe 1 and Probe 2 locations, for which the current flowmeter has been designed. Although uncertainty in probe location can effect a flow measurement, it is assumed that the probes in the simulation are placed exactly at the manufacturer's specified position. The pipe Reynolds number Re_D in this equation is defined as

$$Re_D = \frac{4q_m}{\pi\mu D}. \tag{6}$$

Mass flow rate q_m is calculated from Eqn. (4), which is a nonlinear equation for q_m, since C_d in the right-hand side depends on q_m implicitly through the Reynolds number, see Eqn. (5). Therefore, Eqn. (4) requires an iterative scheme to solve. The convergence criteria is taken to be $(q_m^{i+1} - q_m^i)/q_m^{i+1} \leq 10^{-10}$. Diverged or multiple solutions were not found in the regimes tested.

While the measured mass flow rate q_m is calculated from the measured pressure differential, the nominal mass flow rate specified in the simulations can be computed as $Q_m = \iint_\Omega \rho u(r,t)\, d\Omega$ where $u(r,t)$ is the inlet velocity corresponding to either a plug $(u(r,t) = v(t))$, or a parabolic inflow $(u(r,t) = v(t)(1 - r^2/R^2))$, R is the pipe radius, and Ω is the pipe inlet cross section area. Dependence of the inlet velocity on time is introduced to describe the unsteady mass flow cases considered later in the paper. $v(t)$ is constant when the steady mass flow cases are considered in the first part of the paper. The error between the two values, $(q_m - Q_m)/Q_m \times 100\%$, measures the accuracy of the flow rate measurements with the modeled flowmeter. The Reynolds number based on the nominal flow rate

$$Re = \frac{4Q_m}{\pi \mu D} \tag{7}$$

can also be defined and will be used as a true Reynolds number in the subsequent plots. Re_D and Re will be close to each other, where the error in the flowmeter measurements is small. For the purpose of aligning with standard industrial practices, the mass flow rate q_m or Q_m are converted to cubic feet per hour (SCFH) assuming that the density of the natural gas is 0.7 ($\mathrm{kg\,m^{-3}}$) at standard condition.

RESULTS

Steady Mass Flow Conditions

We will first describe the results obtained at the steady mass flow conditions, i.e. when the inlet velocity v is not varying in time. For these simulations, the fluid was at rest initially (zero flow initial conditions), and a constant mass flux at the inlet was suddenly applied.

Flowrate Measurements According to Pressure Probe 2 The flowmeter Eqn. (4) is nominally accurate for Reynolds numbers greater than 4000 under fully developed flow condition. For flowmeter calibration in most industrial piping systems, like natural gas transportation in power plant, a honeycomb flow conditioner is commonly used to eliminate the swirl and the flow asymmetry. It is usually installed around 10D upstream of the orifice flowmeter to promote a fully developed flow when it arrives the orifice flowmeter. The hydrodynamic entrance length is conventionally estimated as 10D for turbulent flows in most practical engineering applications [14]. This implies that if the flow is in a turbulent region, elongating the entrance would not make a significant difference in the velocity profile.

However, in industrial pumps and piping systems, lower Reynolds numbers are achieved frequently during start-up and shut-down. For laminar flows, a hydrodynamic entrance length is significantly longer, estimated as $0.05Re_D$ from a plug flow [14], which, for example, equals to $50D$ for a Reynolds number $Re_D = 1000$, which is in a laminar regime. With that in mind, the approach flow condition that the orifice flow meter sees in practice, might be far from being fully developed, especially in the laminar regimes.

For these conditions, industry still uses Eqn. (4) which has been calibrated for high Reynolds number flow and a fully-developed profile. This leads to a large error in the flow rate measurements at low Reynolds numbers. The error could either come from an empirical equation itself or from an unknown flow condition. To quantify these errors, a set of simulations with varying Reynolds numbers between Re=100 and 10000, have been conducted with a different upstream length and inlet boundary conditions.

To illustrate various possible flow conditions that can happen in a realistic environment, two extreme cases are considered for constructing two error bounds. The upper signed error bound comes from the results with a plug inflow and a very short (2.5D) upstream development length. The lower signed error bound comes from a fully developed parabolic inflow. With the parabolic inflow, the upstream length does not significantly influence the results in the cases investigated. As a verification, we have performed simulations with both 2.5D and 5D upstream pipe lengths and found no difference in the results with the parabolic inflow with the same numerical method (Nek5000), which is reflected in Fig. 2. A development length influences the results, but only slightly, when we go from 2.5D to 5D upstream length with the plug inflow, see Fig. 2.

In Fig. 2, the results from Re=500, 1000, 2000, 4000, 10000 DNS or RANS simulations with ANSYS-Fluent using both plug and parabolic inflow with the upstream length of 3D, and Re=100, 500, 1000, 1500, 2000, 2500, 3000, 3500, 4000, 5000, 10000 DNS or LES simulations with Nek5000 using two different upstream lengths and two inlet conditions (plug and parabolic) are presented. Data was acquired when the flow reached a steady state condition from the quiescent initial state, determined by the state when the pressure difference between the inlet and outlet ceases to fluctuate significantly.

Fig. 2 shows the combined effect of the accuracy of the empirical equation for mass flow rate calculation, but also the effect of the approach flow condition, as well as the numerical accuracy and mesh resolution of the codes, and needs to be interpreted carefully. First observation is that both Nek5000 and ANSYS-Fluent show remarkably good agreement for the mass flow rate error estimation in all the Reynolds number regimes considered, and provide confidence in numerical results. Second observation is that, as expected, both codes show relatively low errors at high Reynolds numbers, while very large errors at low

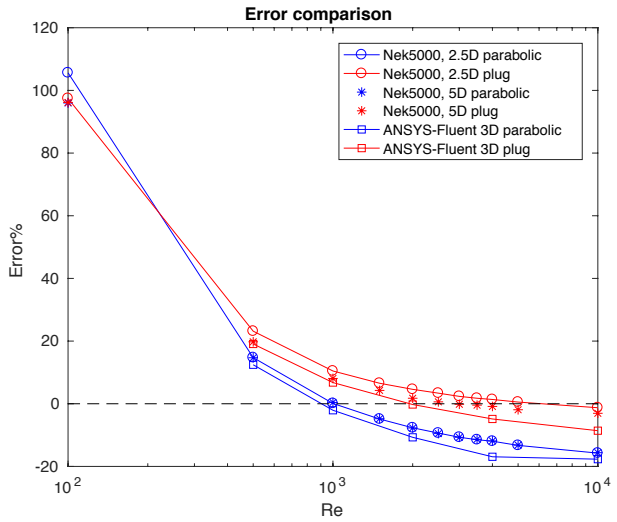

FIGURE 2. RELATIVE ERROR COMPARISON BETWEEN ANSYS-FLUENT AND NEK5000 IN STEADY-STATE REGIME.

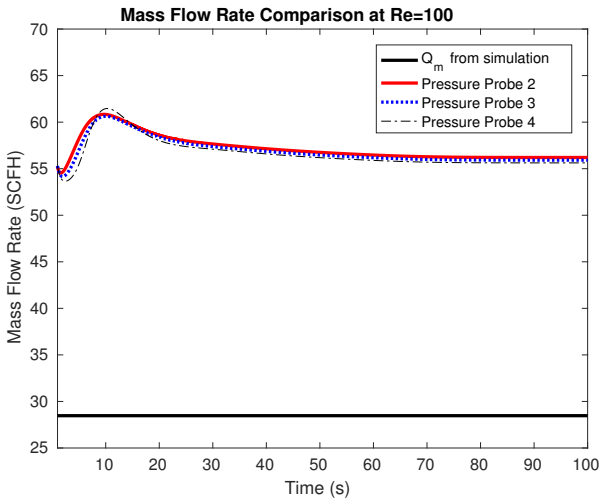

FIGURE 3. THE MASS FLOW RATE COMPARISON FROM DIFFERENT PRESSURE PROBES AT RE=100 WITH 2.5D UPSTREAM PLUG INLET. THE ACTUAL FLOW RATE $Q_m = 28.47$.

Reynolds numbers, confirming the fact that indeed the empirical mass flow rate equation in its original form is not suited for low Reynolds numbers. Slight downward shift of ANSYS-Fluent versus Nek5000 results at higher Reynolds numbers is a manifestation of numerical resolution effects where RANS calculations on coarser grids result in slight underestimation of a mass flow rate contributing to a slight negative error compared to Nek5000 results. We would also like to comment on the difference between parabolic and plug inflow. At low Reynolds numbers of $200 < Re < 1000$, parabolic profile is a better approximation of a fully-developed flow condition and thus gives the smaller errors. At higher Reynolds numbers, when the flow transitions to turbulent, the fully-developed mean pipe flow profile steepens and starts resembling a plug flow closer than a parabolic flow, which explains why the plug inlet results start showing smaller errors, which are in fact close to zero for the grid-resolved results with Nek5000 at Reynolds numbers higher than 2000. Both codes show consistent trends with the inlet conditions, albeit, again, ANSYS-Fluent has slightly higher errors due to mesh resolution. At very low Reynolds numbers of 100, the error coming from the empirical equation itself is so large, close to 100%, that the trends due to the difference in inlet conditions are obscured by the errors. Having demonstrated an overall consistency of numerical results produced by the two codes, in the rest of the paper we will resort to the data obtained by a higher-order code Nek5000 and on a finer mesh compared to ANSYS-Fluent, to make sure that the fluctuating fields are properly resolved, especially in unsteady flow regimes considered later.

Mass Flow Rate Comparison Between Different Pressure Probes In Fig. 2, the pressure difference is calculated from pressure Probes 1 and 2. This section is devoted to estimating the uncertainty to the downstream pressure probe location. Consequently, the flow rate obtained from measuring the pressure differential involving Probes 3 and Probes 4, respectively, will be compared with the flow rate calculated from Probe 2 (upstream pressure Probe 1 is remained fixed at the wall). Two mass flow rate calculations at Re=100 and Re=3500 with 2.5D plug inlet are shown in Fig. 3 and Fig. 4 to determine whether the pressure from different probe locations affects the results. It can be seen that for the two Reynolds numbers presented, the measurement results obtained from different probes vary insignificantly. The cases of other Reynolds numbers were also analyzed by using different probes yielding a similar conclusion, they are however not shown here for conciseness. The case of Re=100 results in an overall mass flow rate difference from different probes of less than 1 (SCFH) which amounts to approximately 1% error at this flow rate compared to almost a 100% error caused by the inconsistency of the orifice flow equation at this very low Re (see Fig. 2). For Re=3500, the difference in mass flow rate obtained from different probes is indistinguishable at steady state. Thus, it was concluded that the uncertainty to the probe location is minimal in these flow regimes, and should not be the issue of concern for engineering practitioners.

Error Correction at Low Reynolds Numbers According to Fig. 2, using Eqn. (4) causes a high relative error when the Reynolds number is low, that is less than ~ 1000. Since there does not seem to be any evidence of unsteadiness or vortex shed-

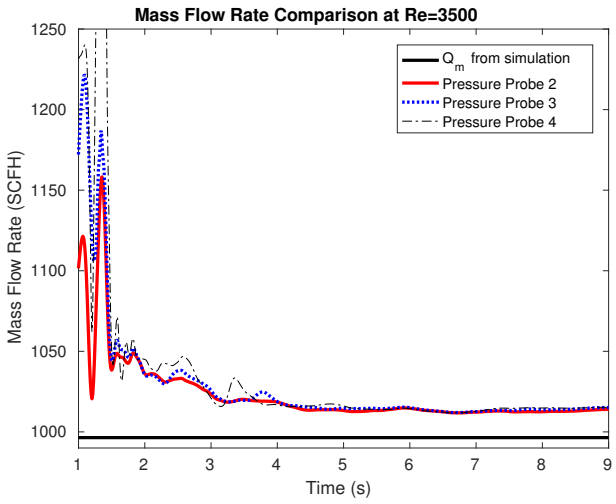

FIGURE 4. THE MASS FLOW RATE COMPARISON FROM DIFFERENT PRESSURE PROBES AT RE=3500 WITH 2.5D UPSTREAM PLUG INLET. THE ACTUAL FLOW RATE Q_m=996.44.

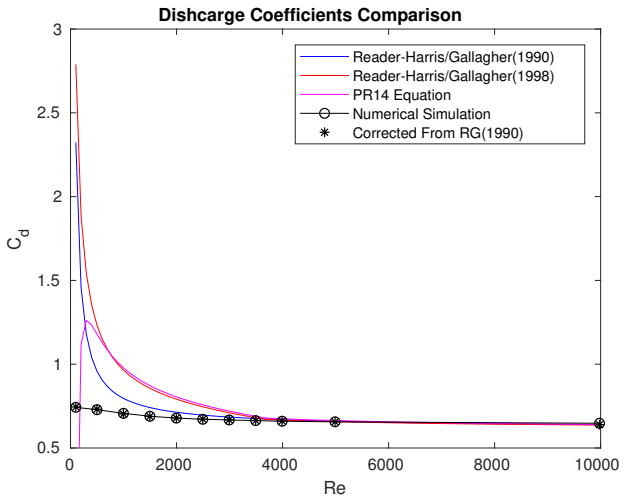

FIGURE 5. THE DISCHARGE COEFFICIENT FROM VARIOUS EMPIRICAL EQUATIONS AND FROM SIMULATION VS. RE FROM 100 TO 10000.

ding below $Re = 1000$, and uncertainty to the probe location is minimal as described above, the most likely cause of error is a poor fit of the Eqn. (4) for the low Reynolds number cases, which can be corrected for. Since the relative error from 2.5D upstream with plug inflow is quite small when $Re > 4000$ consistent with the orifice flow meter specifications, parabolic profile indeed is rare in practical situations due to either a very long development length required in laminar flows, or strong deviations of the mean profile from a parabolic shape in turbulent flows, and the fact that the error difference between two boundary conditions is small at low Reynolds numbers, we incline to correct the empirical Eqn. (4) with the presented orifice geometry based on the results from the upper error bound, i.e. 2.5D upstream with plug inlet.

In Fig. 5, various discharge coefficients computed from different empirical equations are compared with the one from numerical simulation assumed as the "correct" values. Here we only correct Reader-Harris/Gallagher (1990) equation. As the "correct" C_d from simulation could be directly computed from Eqn. (4) by replacing q_m with Q_m, the difference between two C_d can be fitted as a function of Re_D

$$\Delta C_d(Re_D) = \begin{cases} 357 Re_D^{-1.175} - 0.01294; & Re_D \leq 10000 \\ 0; & Re_D > 10000 \end{cases}. \quad (8)$$

Notice that the exact form of the correction $\Delta C_d(Re_D)$ would depend on a particular geometry. This can potentially be merged into a single correction formula across the geometries in a format similar to the empirical equation itself, however obtaining such a universal correction was not the focus of this paper. Once the correction is known, the Reader-Harris/Gallagher (1990) equation valid over all Reynolds numbers can be written as

$$q_m = (C_d - \Delta C_d(Re_D)) E_v Y (\frac{\pi}{4}) d^2 \sqrt{2 g_c \rho \Delta p}. \quad (9)$$

Unsteady Mass Flow Conditions

In the previous section, we investigated the error in orifice flow rate measurements at steady mass flow conditions and proposed a correction for low flow rates which helps to obtain accurate flowmeter readings even at low Reynolds numbers. However, it is often encountered in practice, that the incoming mass flux is varying in an unsteady manner, such as during the start-up and shut-down conditions, or during the opening or closing the valve for maintenance purposes. The unsteady operations can also effect the accuracy of the flow rate measurements, and the current section is devoted to investigation of these effects. All the unsteady cases here are simulated with 2.5D upstream and plug inflow as the focus shifts.

The description of the unsteady test cases The unsteady test cases are designed to simulate the ramp-up conditions that can occur during, for example, a gas turbine start-up process in industrial utilities. To achieve this condition, the inlet velocity v is ramped from its original value v_1 to a higher value v_2 over the duration of a ramp-up time t_{ramp}. The simulations begin from a fully developed flow condition based on the Reynolds number corresponding to a starting inlet velocity v_1. The ramp-up occurs between the time t_1 and t_2, after which the inlet velocity remains constant and equal to v_2 for the duration of the simulations. The ramp function was designed which is a third order polynomial in

TABLE 1. RAMP FUNCTION PARAMETERS FOR UNSTEADY CASES

Case	t_1(s)	t_2(s)	v_1(mm/s)	v_2(mm/s)	Re_1	Re_2
A	5	7	5	12.5	1000	2500
B	5	7	7.5	12.5	1500	2500
D	5	7	10	12.5	2000	2500
D	5	9	5	12.5	1000	2500
E	5	7	1.25	3.125	250	625

time and has a zero slope at both the initial time t_1 and final time t_2 (corresponding to zero initial and final acceleration). The time-dependent inlet velocity $v(t)$ for the duration of the simulations can then be described by the following equation

$$v(t) = \begin{cases} v_1 & 0 \le t < t_1, \\ a(t-t_1)^3 + b(t-t_1)^2 + c & t_1 \le t \le t_2, \\ v_2 & t_2 < t. \end{cases} \quad (10)$$

The description of the ramp-up parameters corresponding to several simulated unsteady cases are provided in Table 1, while the coefficients a, b, c are obtained from fitting the corresponding third-order polynomials.

Error From Start-up Mass flow rate comparison between the actual and measured flow rates in different probes is shown in Figs. 6 and 7 for selected test cases, Case A and E, both uncorrected and corrected (according to Eq. 9) are presented. It is seen that while correction definitely helps to get rid of a systematic bias in the measurements (by shifting the profiles down closer to the actual value), a significant error associated with the velocity ramp still persists. This error can be attributed to a transient vortex shedding, that occurs due to a sudden flow influx resulting in a pressure ramp during unsteady conditions [15]. Such vortex shedding is visualized in Figs. 8–10 for Case A. These figures show a snapshot of the pressure field that illustrates the vortex formation. A distinct high pressure region is formed at the initial time of the ramp-up in the centerline region of the flow past the orifice, resulting in a low pressure region near the wall which causes the primary vortex to form. The low pressure region affects the pressure probes at the wall and artificially increases the measured pressure differential resulting in the overestimation of the measured flow rate (up to 15% in Case E). In Case A, secondary vortex shedding also occurred after the passage of the primary vortex, which is characterized by a periodic shedding of the weaker vortices as can be seen in Fig. 8 at time t=9 seconds (2

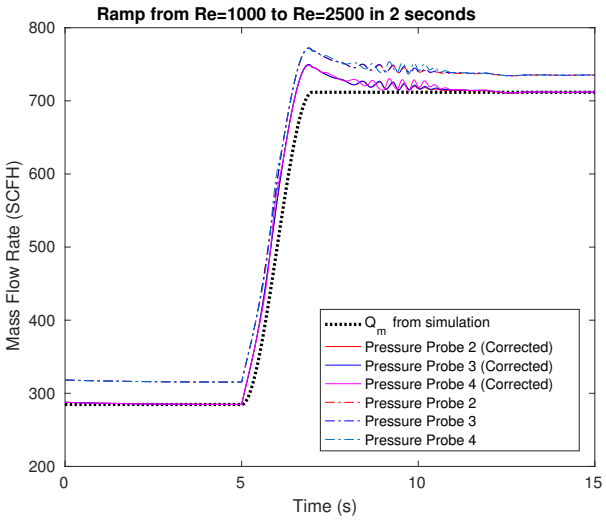

FIGURE 6. MASS FLOW RATE FROM SIMULATION AND PRESSURE PROBES; CASE A.

seconds after the end of the ramp). The secondary vortex shedding results in a fluctuating pressure and thus in a fluctuating flow rate measurement as seen in Fig. 6. The fluctuations associated with the secondary vortex shedding are temporary and last for the duration of approximately 3 seconds in Case A, while they eventually decay and the flow returns to a steady condition. The secondary vortex system was only observed in Case A, which is characterized by the strongest velocity ramp rate $\left(\frac{v_2-v_1}{t_2-t_1}\right)$ among all the cases. While the secondary vortex shedding does not always occur, a primary vortex of a varying strength was detected in all the investigated ramp-up cases, resulting in a transient false positive reading of the flow meter, see an example in Fig. 7 for Case E. Table 2 presents the summary of the observed vortex system parameters and the flow rate measurement errors, where t_p is the time the primary vortex was detection, $\frac{t_p-t_1}{t_2-t_1}$ measures the time of the primary vortex detection since the beginning of the ramp-up versus the duration of the ramp, t_s is the duration of the secondary vortex system, if observed, q_m is the measured flow rate, Q_m is the actual flow rate (in SCFH) at the passage of the primary vortex (corresponding to the largest error), and "Error" is the maximum flow measurement error. It is seen that, while the erroneous measurements in this situation are transient and only last for several seconds, the attainable errors are not insignificant, reaching as mush as 12% in some cases. These errors can bias the bulk statistics of the machinery operations, as well as overestimate the peak consumption, and can lead to inappropriate actions and unstable feedback loops if coupled with real-time control systems.

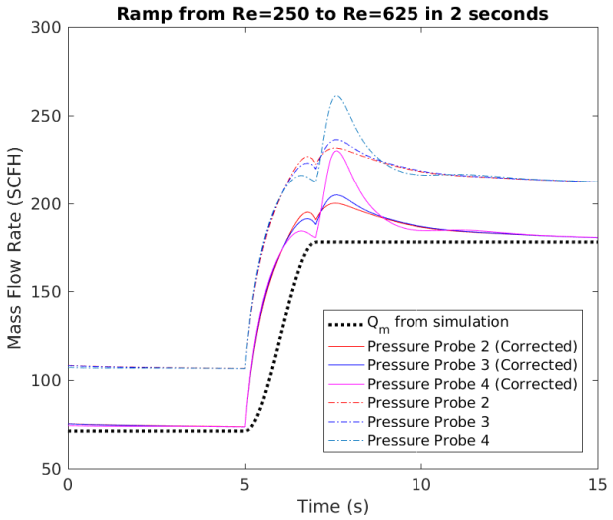

FIGURE 7. MASS FLOW RATE FROM SIMULATION AND PRESSURE PROBES; CASE E.

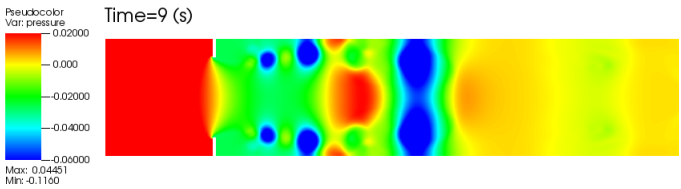

FIGURE 8. SNAPSHOT OF PRESSURE FIELD; CASE A AT TIME=9 S (2 S AFTER THE END OF THE RAMP).

TABLE 2. PROPERTIES OF THE VORTEX SYSTEMS AND MAXIMUM MEASUREMENT ERRORS

Case	t_p(s)	$\frac{(t_p-t_1)}{(t_2-t_1)}$	t_s(s)	$q_m(SCFH)$	$Q_m(SCFH)$	Error, %
A	6.8985	0.9492	2.58	750.24	708.55	5.884%
B	6.9075	0.9538	N/A	737.71	709.97	3.907%
C	6.9085	0.9542	N/A	723.76	710.88	1.812%
D	8.8455	0.9613	N/A	733.37	709.88	3.309%
E	7.554	1.2770	N/A	199.28	177.91	12.01%

CONCLUSION

This paper has investigated the accuracy of the conventional Bernoulli-type orifice flow meters at low Reynolds numbers. Accurate measurements at low flow rates are important for industrial operations, especially in the regimes of start-up and shutdown of the equipment. Via high-fidelity numerical simulations, we have demonstrated that the conventional empirical formula for discharge coefficient by Reader-Harris/Gallagher (1990) [4] is inaccurate a low flow rates, giving the relative error up to 100%

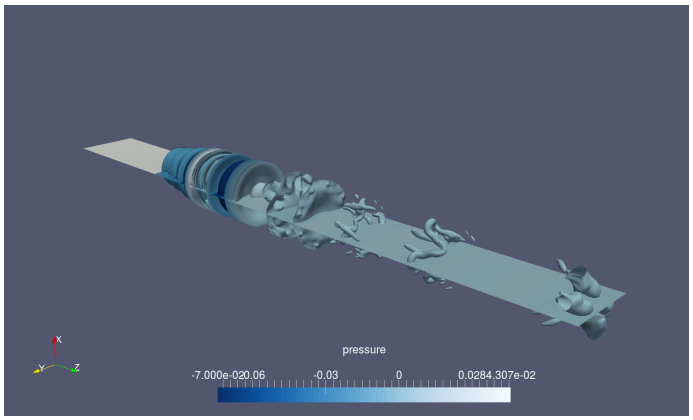

FIGURE 9. ISO CONTOUR OF PRESSURE FIELD; CASE A AT TIME=9 S (2 S AFTER THE END OF THE RAMP).

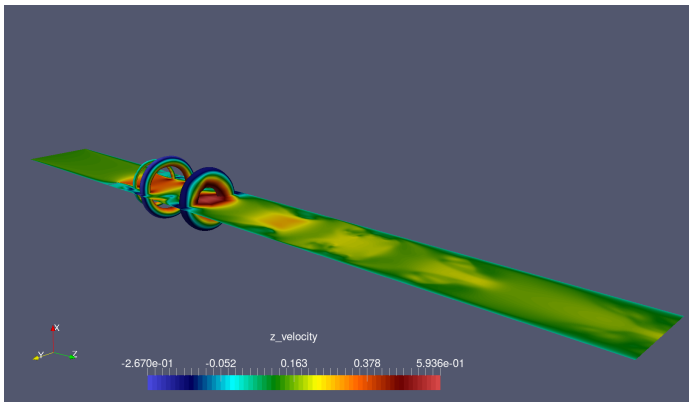

FIGURE 10. ISO VOLUME OF PRESSURE FIELD COLORED BY STREAMWISE VELOCITY; CASE A AT TIME=9 S (2 S AFTER THE END OF THE RAMP).

at Reynolds numbers close to $Re = 100$, which gradually decreases and becomes negligible after $Re = 4000$. To improve the accuracy reading at low Reynolds numbers while keeping a high accuracy at high Reynolds numbers, we have proposed a low Reynolds number correction for this particular orifice geometry, which can potentially be extended to more general geometries.

While the flow measurement error can be corrected by a simple additive correction in steady cases, the situation is more complicated in unsteady cases, for example, the cases featuring the ramp-up of the velocity, such as in the situation of starting up the equipment. It was demonstrated via flow visualization, that in such cases a transient vortex system develops that results in a sudden drop of pressure behind the orifice wall, significantly stronger than the corresponding increase in pressure differential that would otherwise occur during a steady flow with a corresponding mass flow rate. This low pressure region is associated

with a sudden flow influx due to a ramp-up, and results in a significant overprediction of the measured flow rate which in this case can not be corrected by equation. In some cases, a secondary vortex system results in the fluctuations of the measured flow rate associated with the pressure fluctuations due to passing vortices, which eventually die down. Although the identified unsteady flow rate measurements errors are transient and do not last longer than several seconds, they might result in overestimation of both bulk and peak fuel consumption quantities, and can be detrimental if coupled with real-time monitoring and control systems by causing overshoots and unstable feedback in closed-loop operations. While correction of the unsteady errors is beyond the scope of this work, it is important to characterize these errors and make the industry practitioners aware of their nature and their severity.

ACKNOWLEDGEMENTS

The authors of this manuscript gratefully acknowledge the support of Salt River Project Power and Water (SRP) public utility company through a joint research program between SRP and ASU. We are particularly indebted to the SPR project managers Robert Hess, Eric Robinson and Vy Kieu for their advice and sharing their expertise in the industrial utilization of the flow meters.

REFERENCES

[1] Reader-Harris, M., 2015. Orifice Plates and Venturi Tubes. Springer International Publishing.

[2] Lynnworth, L., 1989. Ultrasonic Measurements for Process Control. Academic Press.

[3] Miller, R. W., 1996. Flow Measurement Engineering Handbook, 3 ed. McGraw-Hill Companies.

[4] Gallagher, J. E., 1990. The A.G.A. Report No.3 Orifice Plate Discharge Coefficient Equation. Tech. rep., Calgary, June. Paper presented at the Second International Symposium on Fluid Flow Measurement.

[5] Sigurdson, L. W., and Chapple, D. D., 1998. "A turbulent mechanism for pulsation-induced orifice plate flow meter error". 13th Australasian Fluid Mechanics Conference.

[6] McKee, R. J., 1989. "Pulsation effects on orifice metering considering primary and secondary elements". Proc. of the 22nd Gulf Coast Measurements Short Course.

[7] Varghese, S., Frankel, S. H., and Fischer, P. F., 2007. "Direct numerical simulation of stenotic flows. part 1. steady flow". Journal of Fluid Mechanics, **582**, pp. 253–280.

[8] Deville, M. O., Fischer, P. F., and Mund, E. H., 2002. High-Order Methods for Incompressible Fluid FLow. Cambridge University Press.

[9] Fischer, P., 1997. "An overlapping Schwarz method for spectral element solution of the incompressible Navier-Stokes equations". J. Comp. Phys., **133**, pp. 84–101.

[10] Fischer, P., and Mullen, J., 2001. "Filter-based stabilization of spectral element methods". C. R. Acad. Sci. Paris, **332**, pp. 265–270.

[11] Chatterjee, T., and Peet, Y. T., 2018. "Regularization modelling for large-eddy simulation in wall bounded turbulence: an explicit filtering-based approach". Int. Journal Numer. Methods Fluids.

[12] Doormaal, J. V., and Raithby, G., 1984. "Enhancements of the simple method for predicting incompressible fluid flows". Numerical Heat Transfer, **7**, pp. 147–163.

[13] Menter, F., 1994. "Two-equation eddy-viscosity turbulence models for engineering applications". pp. 1598–1605.

[14] Çengel, Y. A., and Cimbala, J. M., 2006. Fluid Mechanics: Fundamentals and Applications, 1 ed. McGraw-Hill Higher Education.

[15] Brunone, B., Karney, B. W., Mecarelli, M., and Ferrante, M., 2000. "Velocity profiles and unsteady pipe friction in transient flow". J. Water Resour. Plann. Manage., **126**(4), pp. 236–244.